Inorganic Chemistry

Article

pubs.acs.org/IC

Os(II) Phosphors with Near-Infrared Emission Induced by Ligand-to-Ligand Charge Transfer Transition

Jia-Ling Liao,[†] Yun Chi,*[,†] Shih-Hung Liu,[‡] Gene-Hsiang Lee,[‡] Pi-Tai Chou,*[,‡] Hao-Xiang Huang,[§] Yu-De Su,[§] Chih-Hao Chang,*[,§] Jin-Sheng Lin,[∥] and Meu-Rurng Tseng[∥]

[†]Department of Chemistry and Low Carbon Energy Research Center, National Tsing Hua University, Hsinchu 30013, Taiwan

[‡]Department of Chemistry and Center for Emerging Material and Advanced Devices, National Taiwan University, Taipei 10617, Taiwan

[§]Department of Photonics Engineering, Yuan Ze University, Chungli 32003, Taiwan

[∥]Material and Chemical Research Laboratories, Industrial Technology Research Institute, Hsinchu 31040, Taiwan

Supporting Information

ABSTRACT: Heating of $Os_3(CO)_{12}$ with 6 equiv of 2-(3-(trifluoromethyl)-1*H*-1,2,4-triazol-5-yl) pyridine (fptzH) in refluxing diethylene glycol monomethyl ether, followed by sequential treatment with stoichiometric Me_3NO and addition of $PPhMe_2$, afforded two isomeric mixtures of red-emitting $[Os(fptz)_2(PPhMe_2)_2]$ (**1T** and **1C**), for which the notations T and C stand for the *trans* and *cis*-oriented fptz chelates, respectively. Alternatively, preparation of Os(II) complex using a 1:1 mixture of 5,5′-di(trifluoromethyl)-3,3′-di-1,2,4-triazole ($dttzH_2$) and 2,2′-bipyridine (bpy), instead of fptzH, gave isolation of a mononuclear Os(II) complex $[Os(bpy)(dttz)(CO)_2]$ (**2**) in moderate yield. Replacement of CO with $PPhMe_2$ on **2** afforded near-infrared (NIR)-emitting Os(II) complex $[Os(bpy)(dttz)(PPhMe_2)_2]$ (**3**). The single-crystal X-ray structural analyses were executed on **1C**, **2**, and **3** to reveal the structural influence imposed by the various chelates. The photophysical and electrochemical properties were measured and discussed using the results of density functional theory (DFT) and time-dependent DFT calculations. Complex **3** is selected as the dopant to probe its electroluminescent properties by fabrication of the NIR emitting organic light-emitting diodes.

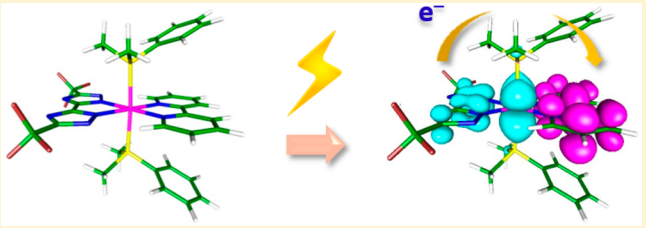

INTRODUCTION

Transition-metal complexes with room temperature phosphorescence have received a wealth of attention during the past two decades due to their profound photophysical fundamentals[1−8] and potential applications in the organic light-emitting diodes (OLEDs) suited for full color displays,[9−11] or even white-emitting OLEDs for solid-state lighting.[12−15] These phosphors exhibit efficient visible emission, that is, with color spanning from blue to red. Parallel to this endeavor, another class of materials being of great interest is the near-infrared (NIR) phosphors, that is, those with emission peak wavelength beyond 700 nm,[16−18] which is important for applications in the fields of optical signal processing, night-vision target identification,[19] luminescent sensing,[20] and photodynamic therapy.[21−24] In contrast to the primary NIR material design using donor−acceptor-based organics,[25,26] NIR phosphors have been successfully obtained using the Pt(II) metal complexes, for which both the extended π-conjugation on the peripheral chelate or the efficient $\pi\pi$ stacking occurring in the solid state were two strategies for induction of efficient, longer wavelength emission. As such, many efficient NIR-emitting OLEDs based on the Pt(II) complexes were demonstrated.[27−31] Most notably, NIR electroluminescence (EL) with λ_{max} = 772 nm and external quantum efficiency (EQE) of 5.0% at 1 mA·cm^{-2} were reported for tetrabenzoporphyrin Pt(II) phosphor,[32] while a further improvement in maximum EQE to 9.2% for OLEDs with similar emission peak maxima was observed for the relevant Pt(II) complex with much bulky 3,5-di-*tert*-butylphenyl substituents.[33] Other effective designs giving the NIR emission at room temperature (RT) involves the Ru(II) complexes displaying a π-bonded quinonoid electron-donating entity,[34] as well as heteroleptic Ir(III) complexes with polyaromatic cyclometalates.[35−37]

In this study, we continue our efforts in developing NIR emitting Os(II) phosphors, which previously employed the highly conjugated isoquniolinyl azolate chelate and equivalents to lower the excited state energy level.[38,39] Since the Os(II) complexes possess an octahedral geometry, we can rule out the contribution from the intermolecular $\pi\pi$ stacking interaction, as observed in the square planar Pt(II) complexes, to simplify the tactics. Herein, we report on a new class of Os(II) complex with formula $[Os(bpy)(dttz)(PPhMe_2)_2]$ (**3**) flanked by chelating 2,2′-bipyidine (bpy) and 3,3′-bi-1,2,4-triazolate (dttz), so that we can take advantage of both synthetic simplicity and ligand-to-ligand charge transfer (LLCT)

Received: June 20, 2014
Published: August 20, 2014

   dx.doi.org/10.1021/ic501474r | *Inorg. Chem.* 2014, 53, 9366−9374

transition for lowering the emission gap.[40] To precisely address the LLCT contribution (i.e., from bitriazolate to bipyridine) in the lower lying excited state, we also made an effort to isolate and fully characterize a cis-substituted 3-(2-pyridyl)-1,2,4-triazolate Os(II) complex $[Os(fptz)_2(PPhMe_2)_2]$ (**1C**), for which its coordination arrangement is distinctive from the dominated trans-substituted complex (**1T**), and both belong to a class of red-emitting Os(II) phosphors with the lowest energy excited state being dominated by metal-to-ligand charge transfer (MLCT).[39,41] Moreover, the isomer **1C** is structurally relevant to the recently reported Os(II) complex (**c-Os**) with a tetradentate chelate formed by linking two 2-pyridyl pyrazolate moieties with a phenylimido fragment (see Chart 1).[42]

Chart 1. Structural Drawings of Os(II) Complexes 1T, 1C, c-Os, and 3

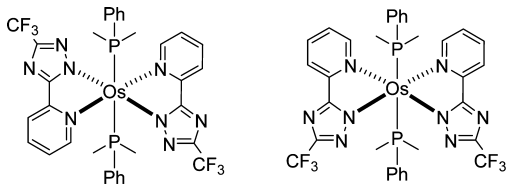

Syntheses, structure characterization, and spectroscopic comparison among these closely related Os(II) complexes **1C** and **1T** and **3** were then performed. Details of our experimental results and corresponding discussions are elaborated as follows.

RESULTS AND DISCUSSION

Syntheses and Characterization. It has been reported that 2-(3-(trifluoromethyl)-1*H*-1,2,4-triazol-5-yl) pyridine (fptzH), was capable to react with $Os_3(CO)_{12}$ in refluxing diethylene glycol monomethyl ether (DGME) to afford the dicarbonyl complex $[Os(fptz)_2(CO)_2]$ (see Chart 2 for structural drawing).[43] Then, the *in situ* treatment of $[Os(fptz)_2(CO)_2]$ with Me_3NO and addition of $PPhMe_2$ gave isolation of all *trans*-$[Os(fptz)_2(PPhMe_2)_2]$ (**1T**) as the major product. With an aim to further explore this reaction, we proceeded to isolate the minor product *cis*-$[Os(fptz)_2(PPhMe_2)_2]$ (**1C**), for which the dual ftpz chelates adopted the distinctive cis-orientation.[42] Furthermore, after the successful preparation of a potentially dianionic chelate 5,5′-di(trifluoromethyl)-3,3′-di-1,2,4-triazole ($dttzH_2$),[44] we became interested in studying the cross-coupling of both 5,5′-di(trifluoromethyl)-3,3′-di-1,2,4-triazole ($dttzH_2$) and 2,2′-bipyridine (bpy) on the coordination sphere of Os(II) metal atom. Hence, the respective dicarbonyl complex $[Os(bpy)(dttz)(CO)_2]$ (**2**) as well as $[Os(bpy)(dttz)(PPhMe_2)_2]$ (**3**) were isolated using the ligand coordination and the subsequent substitution, respectively. These Os(II) complexes **1C**, **2**, and **3** were purified by column chromatography and recrystallization, followed by routine mass spectrometry, IR and NMR spectroscopies, and elemental analyses. The key spectroscopic data were the highly downfield ^1H NMR signals at δ 10.12 (d, J = 5.6 Hz) and 10.35 (d, J = 5.6 Hz) for complexes **1T** and **3**; both are attributable to the intramolecular C−H···N hydrogen bonding between pyridine and triazolate fragments. In sharp contrast, complexes **1C** and **2** showed much less downfield ^1H NMR signals at δ 9.12 (d, J = 5.6 Hz) and 9.40 (d, J = 5.6 Hz), due to the geometrical constraint imposed by these N-chelates that prevented the formation of this intramolecular H-bonding.

The single-crystal X-ray diffraction studies were also executed, for which the perspective view and selected bond lengths and angles are shown in Figures 1−3. As can be seen, all

Chart 2. Structural Drawings of $[Os(fptz)_2(CO)_2]$ and 2

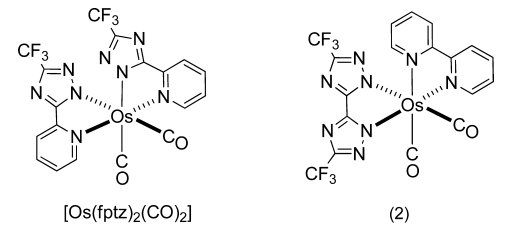

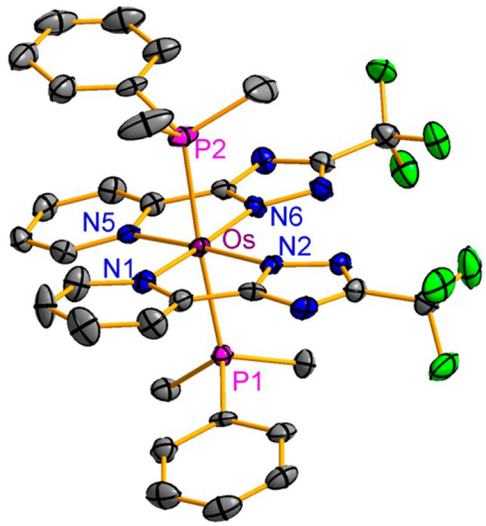

Figure 1. Structural drawing of **1C** with thermal ellipsoids shown at 30% probability level; selected bond distances: Os−N(2) = 2.060(3), Os−N(6) = 2.056(3), Os−N(1) = 2.133(3), Os−N(5) = 2.130(3), Os−P(1) = 2.3404(11), and Os−P(2) = 2.3398(10) Å; bond angles: ∠P(1)−Os−P(2) = 176.53(4), N(1)−Os−N(2) = 76.08(13), and N(5)−Os−N(6) = 76.14(13)°.

Os(II) complexes adopt the distorted octahedral arrangement with phosphines located at the trans-disposition and possessing essentially identical Os−P distances for both **1T** and **3**, while carbonyl ligands in **2** are residing at the cis-deposition, for minimizing the trans-competition. Concomitantly, the Os−N(tz) distances (2.060(3) and 2.056(3) Å) of **1C** are shorter than the Os−N(py) distances (2.133(3) and 2.130(3) Å). This pattern is identical to those observed in structurally characterized *trans*-$[Os(fppz)_2(PPh_2Me)_2]$,[43] showing the existence of stronger Os−N interaction for the anionic triazolate (or pyrazolate) than that of the neutral pyridyl fragment, which is due to the Coulomb attraction between positive charged Os(II) metal center and anionic chelate. For

dx.doi.org/10.1021/ic501474r | Inorg. Chem. 2014, 53, 9366−9374

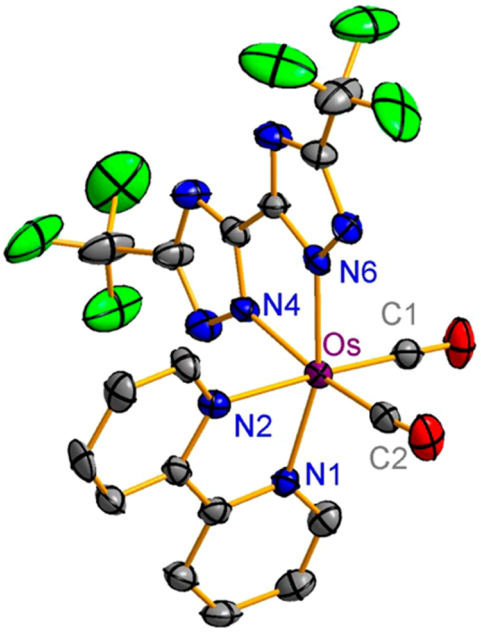

Figure 2. Structural drawing of **2** with thermal ellipsoids shown at 50% probability level; selected bond distances: Os–N(1) = 2.090(4), Os–N(2) = 2.107(5), Os–N(4) = 2.105(4), Os–N(6) = 2.079(4), Os–C(1) = 1.877(6), and Os–C(2) = 1.894(6) Å; bond angels: ∠C(1)–Os–C(2) = 90.6(2), N(1)–Os–N(2) = 77.79(18), and N(4)–Os–N(6) = 75.96(17)°.

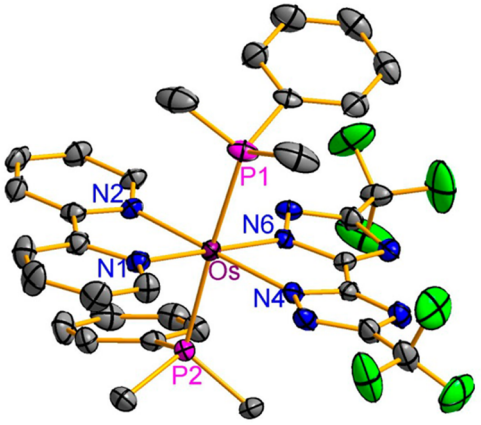

Figure 3. Structural drawing of **3** with thermal ellipsoids shown at 50% probability level; selected bond distances: Os–N(1) = 2.065(4), Os–N(2) = 2.057(4), Os–N(4) = 2.093(4), Os–N(6) = 2.086(4), Os–P(1) = 2.3432(13), and Os–P(2) = 2.3403(12) Å; bond angels: ∠P(1)–Os–P(2) = 176.91(4), N(1)–Os–N(2) = 77.59(15), and N(4)–Os–N(6) = 75.50(14)°.

complex **2**, all Os–N distances are gradually turned equal, despite of the small elongation of Os–N distances that were induced by the trans-influence of cis-carbonyl ligands. In the meantime, a reversal of Os–N distances (Os–N(4) = 2.093(4) and Os–N(6) = 2.086(4) Å) was observed for the anionic triazolates versus that of the pyridyl fragments, Os–N(1) = 2.065(4) and Os–N(2) = 2.057(4) Å. Basically, the longer Os–N distances for the triazolate chelates can be caused by the direct fusion of two five-membered triazolate fragments in forming the 5–5–5-rings bidentate chelate. Thus, the Coulomb interaction cannot fully compensate the internal strain occurred, giving increase of Os–N(tz) distances. It is notable that the closely related 2,6-di(pyrazol-3-yl)pyridine chelate is capable to react with $Os_3(CO)_{12}$ in forming mononuclear Os(II) complex with a maximum of two CO ligands.[45] The analogous 2,2′-biimidazole, also with two fused five-membered rings in forming the bidentate chelate, forms metal complexes with elongated M–N distance, in contrast to more usual bpy chelates that prefer substantially shorter M–N interaction.[46]

Photophysical Properties. The absorption in CH_2Cl_2 and solid-state emission spectra of all Os(II) complexes are shown in Figures 4 and 5, respectively, while Table 1 lists the

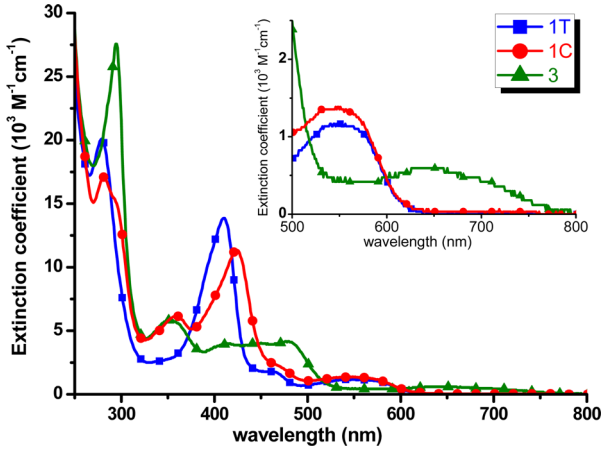

Figure 4. Absorption spectra of Os(II) complexes **1T**, **1C**, and **3** in CH_2Cl_2 at RT.

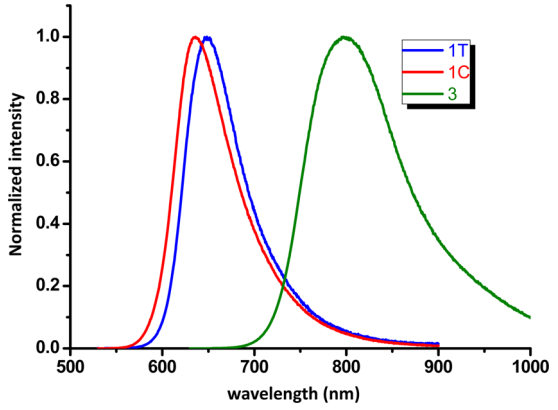

Figure 5. Solid-state emission spectra of Os(II) complexes **1T**, **1C**, and **3** measured at RT.

corresponding numerical data. In general, the strong absorption bands observed at 410 and 424 nm for **1T** and **1C** are assigned to the spin-allowed $^1\pi\pi^*$ transition of fptz chelates. The next lower energy absorption band around ~460 nm can be ascribed to a spin-allowed metal-to-ligand charge transfer transition (^{1}MLCT) mixed with triazolate → pyridyl intraligand charge transfer (^{1}ILCT) transition. The lowest energy band with peak wavelength of ~550 nm and extending beyond 600 nm with relatively small absorptivity is tentatively assigned to the tail of vibronic ^{1}MLCT and ^{1}ILCT transitions mixed with both spin–orbit coupling enhanced $^3\pi\pi^*$ (ILCT) and ^{3}MLCT characters. In comparison to **1T** (or **1C**), complex **3** that possesses mixed bpy and dttz chelates instead of dual fptz chelates lacks ~400 nm absorption band (see Figure 4). This also gives an indirect support for the assignment of fptz $^1\pi\pi^*$ transition (400–420 nm) for **1T** and **1C**. Instead, for **3**, the bpy chelate $^1\pi\pi^*$

dx.doi.org/10.1021/ic501474r | Inorg. Chem. 2014, 53, 9366–9374

Table 1. Selected Photophysical and Electrochemical Properties of Os(II) Complexes

	photophysical data					$E_{1/2}$(V)[a] [ΔE_p (mV)][a]	
	abs. λ_{max} (nm) [ε (10^3 M^{-1} cm^{-1})][b]	PL λ_{max} (nm)[c]	QY (%)[c]	τ (ns)[c]	$k_r \times 10^{-5}$ (s^{-1})[c]	ox. $E_{1/2}$	red. $E_{1/2}$
1T	279 [20.1], 410 [13.8], 462 [1.8], 556 [1.2]	648	50	665	7.52	0.078 [76]	−2.62 [124]
1C	281 [17.1], 356 [6.1], 424 [11.3], 468 [2.2], 546 [1.4]	632	53	776	6.83	0.087 [80]	−2.56 [118]
3	294 [27.5], 351 [5.8], 402 [3.7], 483 [4.1], 614 [0.5]	797	0.16	24	0.67	0.114 [92]	−2.12 [92]

[a]All electrochemical potentials were measured in a 0.1 M $TBAPF_6/CH_2Cl_2$ and tetrahydrofuran solution for oxidation and reduction reaction, and they were reported in volts using Fc/Fc^+ as reference. ΔE_p is defined as E_{ap} (anodic peak potential) − E_{cp} (cathodic peak potential), and these data are quoted in millivolts. The Pt electrode and Au(Hg) alloy were selected as the working electrode of oxidation and reduction processes, respectively. [b]UV−vis spectra were recorded in CH_2Cl_2 at a concentration of 10^{-5} M. [c]Photoluminescence spectra and quantum yields were measured for a powder sample.

transition reveals a peak that is blue-shifted (cf. fptz) to ∼350 nm (see Figure 4). The poorly resolved peaks between 405−483 nm are assigned to the mixed ^{1}MLCT to bpy and ligand-to-ligand charge transfer transition (^{1}LLCT) from dttz to bpy, while the lowest energy band of >600 nm, which has rather small absorption extinction coefficient of $<10^3$ M^{-1} cm^{-1}, is attributed to a ^{3}MLCT process, mixed with a small proportion of ^{3}LLCT character.

To gain more detailed insight into the fundamental bases of the above observed photophysics the time-dependent density functional theory (TD-DFT) calculations were then performed. Key frontier molecular orbitals involved in the first three lower lying transitions are depicted in Figure 6 (for highest occupied

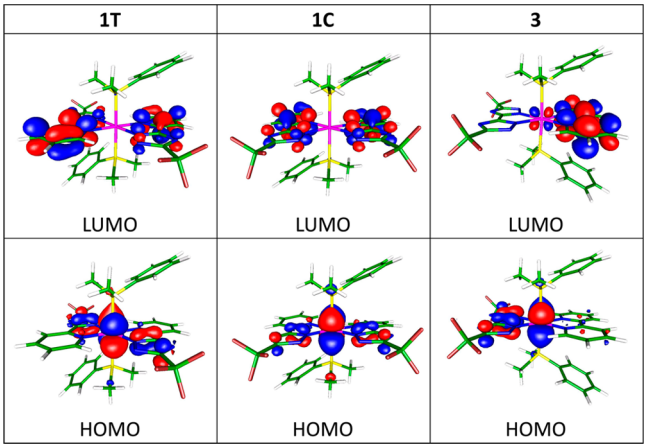

Figure 6. Selected frontier orbitals involved in the lower-lying transition for Os(II) complexes **1T**, **1C**, and **3**.

molecular orbital (HOMO) and lowest unoccupied molecular orbital (LUMO)) and Figures S1−S3 of the Supporting Information for complexes **1T**, **1C**, and **3**. Table 2 displays the calculated energy and orbital analyses of the lowest optical transition for complexes **1T**, **1C**, and **3** in both singlet and triplet manifolds. The calculated wavelengths of the S_0−S_1 transitions for **1T**: 513.3 nm, **1C**: 493 nm, and **3**: 601.6 nm are close to the observed onsets of the major absorption peaks at >420 nm (i.e., the ∼510 nm for **1T** and **1C**, ∼614 nm for **3**) recorded in Figure 4. Moreover, the calculated wavelengths of S_0−T_1 energy gap for **1T**: 543.6 nm, **1C**: 530 nm, and **3**: 654.6 nm are also in agreement with the trend of their corresponding lowest lying absorption band depicted in Figure 4. The trend also qualitatively matches the onset of their phosphorescence spectra around 590, 575, and 705 nm for **1T**, **1C**, and **3**, respectively (see Figure 5). The calculation also faithfully reproduces the slightly higher energy gap for **1C** than its geometric isomer **1T**, similar to that observed in both absorption and emission spectra. Technically, this can be rationalized by the operation of intramolecular H-bonding in **1T**, resulting in a relatively stabilized π^*-orbital on the pyridyl fragment and hence lowered energy gap (cf. **1C**). It is also noteworthy that the calculated $S_0 \rightarrow T_1$ transition probability (oscillator strength) is zero due to its strictly forbidden singlet−triplet conversion under zeroth-order approximation. In reality, however, the $S_0 \rightarrow T_1$ transition of the titled Os(II) complexes should be partially allowed due to the heavy-atom induced spin−orbit coupling, giving the non-negligible transition moment based upon the first-order perturbation theory. The combination of $S_0 \rightarrow S_1$ and $S_0 \rightarrow T_1$ transition rationalizes the experimentally observed spectral onset toward, for example, ∼700 nm for complex **3**.

The $S_0 \rightarrow S_1$ and $S_0 \rightarrow T_1$ optical transitions for complexes **1T**, **1C**, and **3** are assigned to the HOMO → LUMO type of metal-to-ligand charge transfer process, in which the electron density distributions of HOMO are all mainly localized at the center metal Os(II) atom and minor in the 1,2,4-triazolate moiety for **1T** and **1C** and in the 3,3′-di-1,2,4-triazolate part for **3**. The electron density distributions of LUMO for these three studied complexes are mainly placed at the pyridyl moieties of fptz chelates for **1T**, **1C**, and bipyridine for **3** and little at the 1,2,4-triazolate fragments and Os(II) atom for **1T** (or **1C**) and **3**. Therefore, both $S_0 \rightarrow S_1$ and $S_0 \rightarrow T_1$ optical transitions for all complexes are ascribed mainly to MLCT transition (c.f. Table 2), together with a minor contribution from ILCT (**1C** and **1T**) and LLCT (**3**) processes. Accordingly, the charge-

Table 2. Calculated Energy Levels and Orbital Transition Analyses of Os(II) Complexes 1T, 1C, and 3

	state	f (oscillator strength)	λ_{cal} (nm)	assignments	MLCT (%)
1T	T_1	0	543.6	HOMO → LUMO (94%)	62
	S_1	0.0025	513.3	HOMO → LUMO (99%)	65
1C	T_1	0	530	HOMO → LUMO (95%)	65
	S_1	0.0001	493	HOMO → LUMO (99%)	68
3	T_1	0	654.6	HOMO → LUMO (94%)	56
	S_1	0.0021	601.6	HOMO → LUMO (98%)	59

dx.doi.org/10.1021/ic501474r | Inorg. Chem. 2014, 53, 9366−9374

neutral bpy chelate in **3** is expected to have π^* orbital lower in energy than that of fptz ligand in **1T** and **1C**, consistent with the lower energy gap (in terms of absorption and emission) observed for **3** experimentally.

Interestingly, careful frontier orbital analyses of these Os(II) complexes indicate that LUMO+1 of **1T** (or **1C**, see Supporting Information) and LUMO of **3** show a non-negligible contribution of the metal d_π-orbitals. We also realize that the $PPhMe_2$ and triazole moieties, which are all ascribed to the π-acceptor ligands. This, together with the relatively low oxidation potential for the Os(II) atom, leads us to suspect the occurrence of electron donation from metal d_π-orbitals to the empty or antibonding orbital of $PPhMe_2$ and/or triazolate fragments. The net effect is the involvement of metal d_π-orbitals in certain unoccupied orbitals of Os(II) complexes, for example, d_{yz} and d_{zx} orbitals, for which the energetics has been pushed upward due to the perturbed/distorted octahedral symmetry.

Next, as for the photoluminescence (PL), intense red emission was observed for **1T** and **1C** with peak wavelengths at 648 and 632 nm, respectively (see Figure 5). The observed lifetimes of ca. 665 and 776 ns, in combination with the emission quantum yields (QYs) of 0.50 and 0.53, lead us to deduce a radiative lifetime of 7.52 and 6.83 × 10^5 s^{-1} for **1T** and **1C**, respectively, which are much shorter that majority of the relevant Ir(III) phosphors.[47] In sharp contrast, complex **3** with distinctively asymmetric bpy and dttz chelates reveals much red-shifted NIR emission with $\lambda_{max} \approx 800$ nm, together with shortened lifetime of 24 ns and lowered emission QY of only 0.16%. The low QY of **3** is plausibly manifested by the result of energy gap law, for which the great overlap between the emissive S_1 state and high density of ground vibronic states induces fast nonradiative deactivation.[48] In fact, this is also the main reason for us to conduct the measurement of emission in solid state, instead of in solution or fluid state, for reducing any possible large-amplitude vibrational motions and hence to increase emission yield.

Electrochemical Properties. The electrochemical behaviors of Os(II) complexes **1T**, **1C**, and **3** were investigated by cyclic voltammetry using ferrocene as the internal standard, for which the numerical redox data and voltammogram are depicted in Table 1 and Figure 7. During the anodic scan in CH_2Cl_2, all Os(II) complexes exhibited a reversible (or quasi reversible) metal-centered oxidation peak potential in the region of 0.078−0.114 V. The observed anodic potential of **3** at 0.114 V is consistent with the relatively lowest electron density on the Os(II) center and, hence, the increased oxidation potential. Moreover, the trend of oxidation potential for **1T** and **1C** is qualitatively in agreement with the calculated HOMO energy level shown in Table 2. Furthermore, upon switching to the cathodic sweep, apparently, for complexes **1T** and **1C**, this ligand-centered reduction should take place in the π^*-orbital of the fptz chelate, which should be more-or-less identical to each other. On the other hand, according to the theoretical analyses elaborated above, the reduction of **3** should take place at the empty π^*-orbital of neutral bpy chelate, as manifested by their distinctly lowered reduction peak at −2.12 V.

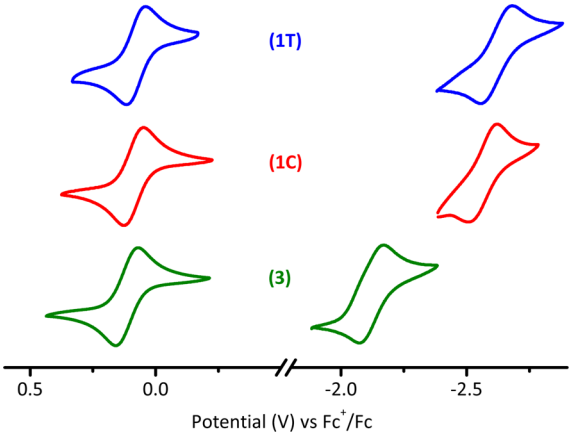

Figure 7. Cyclic voltammograms of the studied Os(II) complexes **1T**, **1C**, and **3**.

OLED Device Fabrication. Complex **3** is selected as a dopant to determine its electroluminescent properties in OLED applications. To ensure efficient exothermic energy transfer, the triplet energy gap (E_T) of host should be wider than that of the guest. Considering the gap of NIR phosphors, many carrier transport materials with adequate triplet energy gaps can be employed as both host and carrier transport materials in NIR OLEDs, leading to a greatly simplified architecture.[49] As such, we examined several commonly used electron transport materials, finding that 3,3',5,5'-tetra[(M-pyridyl)-phen-3-yl]-biphenyl (BP4mPy) satisfied the criteria.[50] To ensure carrier balance, the hole-transport layers (HTLs) were made of 4,4′-bis[*N*-(1-naphthyl)-*N*-phenyl-amino] biphenyl (NPB),[51] which possesses a hole transport mobility (10^{-4} cm^2/V s) comparable to the electron transport mobility (10^{-4} cm^2/V s) of BP4mPy. Figure 8a depicts the chemical structures of the associated materials. Device A consists of a simplified three-layer architecture of indium tin oxide (ITO)/NPB (40 nm)/BP4mPy doped with 15 wt % **3** (30 nm)/BP4mPy (40 nm)/LiF (0.8 nm)/Al (150 nm), for which the configurations and the corresponding energy level diagram are shown in Figure 8b,c.

Furthermore, the emission-absorption overlapping indicates possible energy transfer due to the isoenergetic relationship between the two materials. Considering the energy transfer between host and guest, we examined the PL spectra of BP4mPy as well as the absorption spectrum of **3**. The absorption spectrum of **3** exhibits poor overlap with the PL spectrum of BP4mPy, and thus may result in inferior energy transfer. A similar issue had been previously resolved by using a codoping intermediate which provides a band gap between the host and emitter to create a stepwise energy transfer.[52] In other words, the high-energy exciton formed on BP4mPy could be absorbed by the intermediate and then cascade to NIR-emitting phosphor **3**. According to our previous study of red-emitting complexes,[53] $Os(bpftz)_2(PPh_2Me)_2$ (**4**) offers an appropriate emission spectrum in this approach, which overlaps very well with the absorption spectra of **3**, as shown in Figure 9. Therefore, the modified architecture (i.e., device B) consisted of ITO/NPB (40 nm)/BP4mPy doped with 15 wt % **3** and 0.1 wt % **4** (30 nm)/BP4mPy (40 nm)/LiF (0.8 nm)/Al (150 nm).

The EL characteristics of the tested NIR-emitting OLEDs are shown in Figure 10, and the data are listed in Table 3. Devices A and B exhibited identical spectral profiles as shown in Figure 10a, indicating that the carrier recombination was well confined within the EML and that exciton diffusion to the adjacent layers was avoided. Moreover, only the emission of **3** was observed in device B, which confirms the successful energy transfer from **4** to **3**. On the other hand, the spectral profiles are slightly

dx.doi.org/10.1021/ic501474r | Inorg. Chem. 2014, 53, 9366−9374

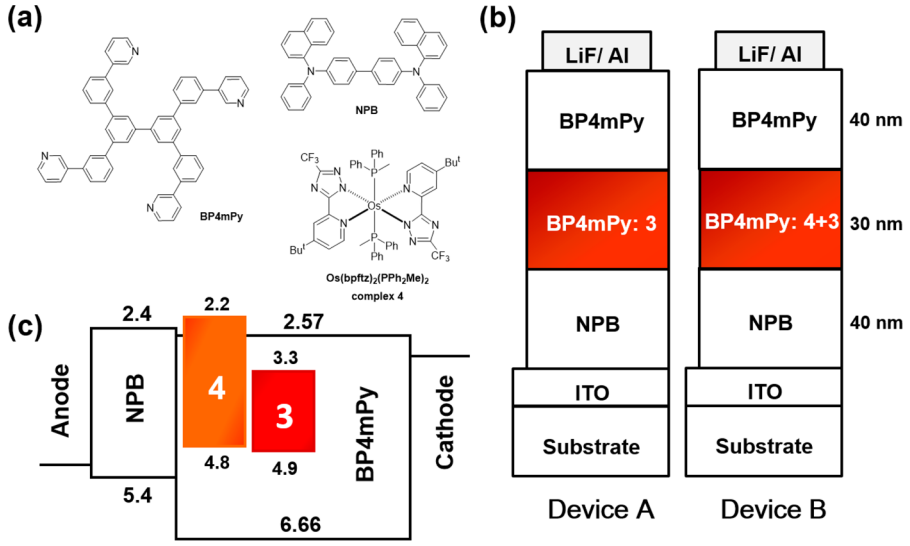

Figure 8. (a) Structural drawing of the materials used in OLEDs; (b) schematic structures and (c) energy level diagram of the tested OLEDs.

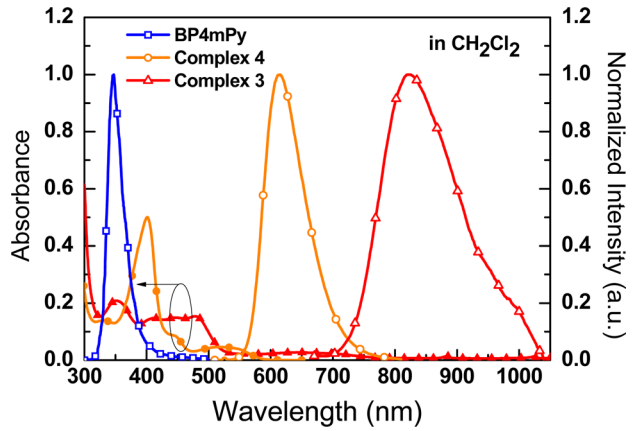

Figure 9. PL spectra and absorption spectra of BP4mPy, and Os(II) complexes **3** and **4** in CH_2Cl_2.

narrower than their respective PL spectra measured in solution, which is the result of the optical influence of the stacked thin films. The peaks of devices A and B are located at ~770 nm, and the full width at half-maximum (FWHM) is approximately 154 nm. Moreover, from the current density–voltage–luminance (J–V–L) curves, the turn-on voltages defined as a sharp rise in current density for devices A and B are respectively found to be only 2.4 and 2.6 V. In contrast to device A, the additional dopant **4** incorporated in device B decreased the current density possibly due to carrier trapping. Devices A and B exhibited respective peak EL efficiencies of 0.057% and 0.067%. The 18% efficiency improvement obtained in device B demonstrates the effectiveness of using complex **4** for stepwise energy transfer. Although neither device provides sufficient efficiency, these results still provide the potentials of this Os(II) phosphor in fabrication of the NIR-emitting OLEDs.

CONCLUSION

In summary, NIR-emitting phosphor **3** was prepared via self-assembling of neutral 2,2′-bipyidine (bpy) and dianionic 3,3′-bi-1,2,4-triazolate (dttz) chelate on the Os(II) metal center. Although the employed synthetic conditions for **3** are identical to those reported for monoanionic 1,2,4-triazol-5-ylpyridine (fptz) chelate, the latter gave isolation of both **1C** and **1T**; their

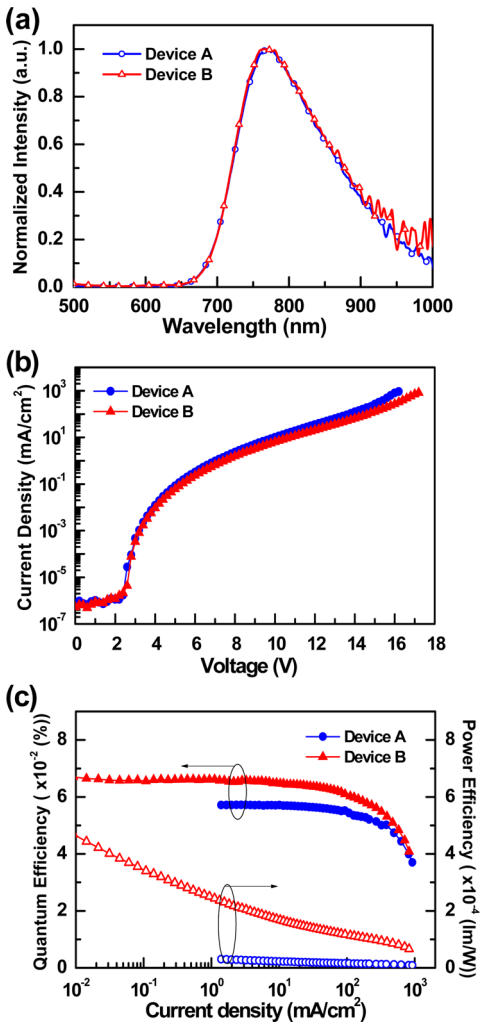

Figure 10. (a) EL spectra of devices A and B, (b) current density–voltage–luminance (J–V–L) characteristics, and (c) external quantum efficiency/power efficiencies vs current density.

photophysical properties are distinctively different, due to the notable variations of the lowest lying excited state characters

dx.doi.org/10.1021/ic501474r | Inorg. Chem. 2014, 53, 9366–9374

Table 3. EL Characteristics of NIR OLEDs with Different Dopants

device	dopant	external quantum efficiency (%)	power efficiency (lm/W)	turn on voltage (V)	light output (μW/cm^2) [@V]
A	**3**	0.057	3×10^{-5}	2.4	2.1 [16.2 V]
B	**3** + **4**	0.067	6×10^{-4}	2.6	10.2 [17.2 V]

that were solely controlled by the assembly of chelates. This methodology can be applied to the syntheses of other third-row transition-metal complexes, that is, giving formation of Pt(II) complexes with a simple combination of neutral and dianionic chelate, or even Ir(III) metal complexes with coexistence of neutral, monoanionic and dianionic trios. Distinctive photophysical properties are anticipated for these new metal phosphors.

In addition, the peak EL efficiency of 0.067% is obtained for our NIR-emitting device, together with an 18% improvement for device having the stepwise energy transfer and exciton diffusion. Also, most of the NIR devices claimed exhibit peak wavelengths of ∼700−800 nm, while the EL emission with peak of >800 nm is rare[34] due to the drastic emission quenching by the congestion of vibrational overtones (energy gap law). The successful fabrication of >800 nm NIR OLED in this study makes feasible the future design of more robust Os(II) complexes toward highly efficient NIR emission of >800 nm.

EXPERIMENTAL SECTION

General Information and Materials. Mass spectroscopy (MS) data were obtained on a JEOL SX-102A instrument operating in electron impact (EI) mode or fast atom bombardment (FAB) mode. ^{1}H, ^{19}F, and ^{31}P NMR spectra were recorded on Varian Mercury-400 or INOVA-500 instruments. Elemental analyses were carried out at the NSC Regional Instrumentation Center at National Chao Tung University, Hsinchu, Taiwan. The 2-(3-(trifluoromethyl)-1,2,4-triazol-5-yl)pyridine (fptzH) was prepared from treatment of 2-cyanopyridine with NH_4Cl in methanol (for *in situ* synthesis of pyridinecarboximidamide hydrochloride), followed by addition of trifluoroacetic acid hydrazide.[54] The 5,5′-di(trifluoromethyl)-3,3′-di-1,2,4-triazole ($dttzH_2$) was obtained from coupling of oxalyl dihydrazide and trifluoroacetamidine in refluxing ethanol, followed by thermal dehydration at atmospheric pressure and vacuum sublimation.[44] All reactions were conducted under N_2 atmosphere using anhydrous solvents or solvents treated with an appropriate drying reagent.

Photophysical Measurement. Detail of measurement of steady-state absorption and emission in both solution and solid state was described in our previous reports.[55] Lifetime studies were measured with Edinburgh FL 920 photon-counting system incorporated with an integration sphere.

Preparation of 1T and 1C. A mixture of $Os_3(CO)_{12}$ (300 mg, 0.33 mmol) and 2-(3-(trifluoromethyl)-1*H*-1,2,4-triazol-5-yl)pyridine (fptzH, 446 mg, 2.09 mmol) in DGME (20 mL) was heated to 190 °C for 24 h under N_2. After it cooled to RT, freshly sublimed Me_3NO (156 mg, 2.08 mmol) was added, and the solution was then heated to 110 °C for 1 h. Then $PPhMe_2$ (301 mg, 2.18 mmol) was added, and the solution was heated to 190 °C for 12 h. After removal of solvent *in vacuo*, the residue was purified by silica gel column chromatography eluting with ethyl acetate (EA)/hexane (2:1), giving dark-red $[Os(fptz)_2(PPhMe_2)_2]$ (**1T**, 532 mg, 0.59 mmol, 60%), and (**1C**, 10 mg, 0.011 mmol, 1%) according to the order of their elution.

Spectral Data of ***1T****.* ^{1}H NMR (400 MHz, d_6-acetone, 294 K): δ 10.12 (d, J = 5.6 Hz, 2H), 7.74 (t, J = 7.8 Hz, 2H), 7.65 (t, J = 7.8, 2H), 7.22 (t, J = 6.6 Hz, 2H), 7.08 (t, J = 7.4 Hz, 2H), 6.91 (t, J = 7.4 Hz, 4H), 6.34 (m, 4H), 0.83 (t, J_{HP} = 3.2 Hz, 6H), 0.65 (t, $^1J_{HP}$ = 3.2 Hz, 6H); ^{13}C NMR (100 MHz, CD_2Cl_2, 294 K): δ 164.77 (s, 2C), 155.21 (s, 2C), 154.32 (q, $^2J_{CF}$ = 36.1 Hz, 2C), 153.50 (s, 2C), 134.60 (s, 2C), 131.36 (t, $^1J_{CP}$ = 21.8 Hz, 2C), 128.73 (s, 2C), 128.24 (t, $^3J_{CP}$ = 4.2 Hz, 4C), 128.23 (t, $^2J_{CP}$ = 4.7 Hz, 4C), 126.40 (s, 2C), 124.32 (s, 2C), 121.22 (q, $^1J_{CF}$ = 269.1 Hz, 2C), 8.48 (t, $^1J_{CP}$ = 14.8 Hz, 1C), 7.90 (t, $^1J_{CP}$ = 14.9 Hz, 1C);^{19}F−{^{1}H} NMR (470 MHz, d_6-acetone, 294 K): δ −63.42 (s, 6F); ^{31}P NMR (202 MHz, d_6-acetone, 298 K): δ −20.65 (s, 2P). MS (FAB, ^{192}Os): m/z 894 (M)$^+$, 756 (M$^+$-PPhMe$_2$), 618 (M$^+$-2PPhMe$_2$); Anal. Calcd for $C_{32}H_{30}F_6N_8OsP_2$: N, 12.55; C, 43.05; H, 3.39. Found: N, 12.54; C, 42.88; H, 3.55%.

Spectral Data of ***1C****.* ^{1}H NMR (400 MHz, d_6-acetone, 294 K): δ 9.12 (d, J = 5.6 Hz, 2H), 7.72 (m, 4H), 7.16 (t, J = 6.6 Hz, 2H), 7.07 (t, J = 7.6 Hz, 2H), 6.90 (t, J = 7.6 Hz, 4H), 6.39 (m, 4H), 0.79 (t, $^1J_{HP}$ = 3.2 Hz, 12H); ^{13}C NMR (100 MHz, CD_2Cl_2, 294 K): δ 165.19 (s, 2C), 155.67 (q, $^2J_{CF}$ = 36.5 Hz, 2C), 155.39 (s, 2C), 151.26 (s, 2C), 135.42 (s, 2C), 132.97 (t, $^1J_{CP}$ = 21.7 Hz, 2C), 128.92 (s, 2C), 128.37 (t, $^3J_{CP}$ = 4.1 Hz, 4C), 128.24 (t, $^2J_{CP}$ = 4.7 Hz, 4C), 123.70 (s, 2C), 121.28 (s, 2C), 121.58 (q, $^1J_{CF}$ = 269.8 Hz, 2C), 8.51 (t, $^1J_{CP}$ = 15.1 Hz, 2C); ^{19}F−{^{1}H} NMR (470 MHz, d_6-acetone, 294 K): δ −63.20 (s, 6F); ^{31}P NMR (202 MHz, d_6-acetone, 298 K): δ −20.93 (s, 2P). MS (FAB, ^{192}Os): m/z 895 (M+H)$^+$, 757 (M$^+$-PPhMe$_2$+H); Anal. Calcd for $C_{32}H_{30}F_6N_8OsP_2$: N, 12.55; C, 43.05; H, 3.39. Found: N, 12.15; C, 43.37; H, 3.78%.

Selected Crystal Data of ***1C****.* $C_{32}H_{32}F_6N_8OOsP_2$; M = 910.80; monoclinic; space group = $P2(1)/n$; a = 10.3275(6) Å, b = 17.2508(11) Å, c = 19.5265(11)) Å, β = 102.2503(14)°, V = 3399.6(4) Å^3; Z = 4; ρ_{calcd} = 1.780 Mg·m^{-3}; $F(000)$ = 1792; crystal size = 0.25× 0.16 × 0.14 mm^3; λ (Mo Kα) = 0.710 73 Å; T = 150(2) K; μ = 3.919 mm^{-1}; 24 806 reflections collected, 7790 independent reflections (R_{int} = 0.0523), GOF = 1.018, final $R_1[I > 2\sigma(I)]$ = 0.0353 and wR_2 (all data) = 0.0737.

Preparation of 2. A mixture of $Os_3(CO)_{12}$ (100 mg, 0.11 mmol), $dttzH_2$ (93 mg, 0.34 mmol) and bipyridine (bpy, 53 mg, 0.34 mmol) in diethylene glycol monomethyl ether (DGME, 10 mL) was heated to 190 °C for 24 h. After it cooled to RT, the solvent was removed under vacuum. The crude was washed with 10 mL of acetone, giving yellow precipitate which was collected by filtration. Recrystallization from a mixture of EA and hexane gave yellow $[Os(bpy)(dttz)(CO)_2]$ (**2**, 89 mg, 0.13 mmol, 40%).

Spectral Data of ***2****.* ^{1}H NMR (400 MHz, d_6-acetone, 294 K): δ 9.40 (d, J = 5.6 Hz, 1H), 8.87 (d, J = 8.0 Hz, 1H), 8.81 (d, J = 8.0 Hz, 1H), 8.49 (t, J = 8.0 Hz, 1H), 8.34 (t, J = 8.0 Hz, 1H), 7.89 (td, J = 6.4 Hz, 1H), 7.73 (t, J = 6.4 Hz, 1H), 7.35 (d, J = 5.2 Hz, 1H); ^{19}F−{^{1}H} NMR (470 MHz, d_6-acetone, 294 K): δ −62.47 (s, 3F), −62.72 (s, 3F); MS (FAB, ^{192}Os): m/z 675 (M-1)$^+$; IR (CH_2Cl_2): ν(CO), 1994, 2058 cm^{-1}; Anal. Calcd for $C_{18}H_8F_6N_8O_2Os$: N, 16.66; C, 32.15; H, 1.20. Found: N, 16.41; C, 32.33; H, 1.45%.

Selected Crystal Data of ***2****.* $C_{21}H_{14}F_6N_8O_3Os$; M = 730.60; monoclinic; space group = $P2(1)/n$; a = 11.3471(6) Å, b = 17.0368(9) Å, c = 12.9426(7) Å, β = 97.8898(14)°, V = 2478.4(2) Å^3; Z = 4; ρ_{calcd} = 1.958 Mg·m^{-3}; $F(000)$ = 1400; crystal size = 0.25 × 0.14 × 0.11 mm^3; λ (Mo Kα) = 0.71073 Å; T = 150(2) K; μ = 5.231 mm^{-1}; 18 957 reflections collected, 5695 independent reflections (R_{int} = 0.0593), GOF = 1.043, final $R_1[I > 2\sigma(I)]$ = 0.0389 and wR_2 (all data) = 0.0847.

Preparation of 3. A mixture of $Os_3(CO)_{12}$ (100 mg, 0.11 mmol), $dttzH_2$ (93 mg, 0.34 mmol) and bipyridine (bpy, 53 mg, 0.34 mmol) in 10 mL of DGME was heated to 190 °C for 24 h. After it cooled to RT, freshly sublimed Me_3NO (52 mg, 0.69 mmol) was added, and the solution was then heated to 110 °C for 1 h. Then $PPhMe_2$ (145 mg, 0.72 mmol) was added, and the solution was heated to 190 °C for 12 h. Finally, the solvent was removed under vacuum, and the residue was purified by silica gel column chromatography eluting with EA/hexane (1:1). Recrystallization from a mixture of EA and hexane gave dark-brown crystals of $[Os(bpy)(dttz)(PPhMe_2)_2]$ (**3**, 155 mg, 0.17 mmol, 51%).

dx.doi.org/10.1021/ic501474r | *Inorg. Chem.* 2014, 53, 9366−9374

Spectral Data of **3**. ^{1}H NMR (400 MHz, d_6-acetone, 294 K): δ 10.35 (d, J = 5.6 Hz, 2H), 7.75 (d, J = 8.0 Hz, 2H), 7.59 (t, J = 7.6 Hz, 2H), 7.31 (t, J = 6.4 Hz, 2H), 7.05 (t, J = 7.6 Hz, 2H), 6.86 (t, J = 8.0 Hz, 4H), 6.31 (m, 4H), 0.77 (t, $^1J_{HP}$ = 3.2 Hz, 12H); ^{13}C NMR (100 MHz, deuterated dimethyl sulfoxide, 294 K): δ 159.52 (s, 2C), 158.07 (s, 2C), 153.78 (s, 2C), 153.34 (q, $^2J_{CF}$ = 35.7 Hz, 2C), 133.57 (s, 2C), 130.59 (t, $^1J_{CP}$ = 21.3 Hz, 2C), 128.21 (s, 2C), 127.73 (t, $^3J_{CP}$ = 4.1 Hz, 4C), 127.43 (t, $^2J_{CP}$ = 4.7 Hz, 4C), 126.40 (s, 2C), 122.58 (s, 2C), 133.57 (q, $^1J_{CF}$ = 268.7 Hz, 2C), 7.20 (t, $^1J_{CP}$ = 15.0 Hz, 2C); ^{19}F–{^{1}H} NMR (470 MHz, d_6-acetone, 294 K): δ −63.20 (s, 6F); ^{31}P NMR (202 MHz, d_6-acetone, 298 K): δ −19.29 (s, 2P). MS (FAB, ^{192}Os): m/z 894 (M^+), 756 (M^+-$PPhMe_2$), 618 (M^+-2$PPhMe_2$); Anal. Calcd for $C_{32}H_{30}F_6N_8OsP_2$: N, 12.55; C, 43.05; H, 3.39. Found: N, 12.72; C, 42.84; H, 3.74%.

Selected Crystal Data of **3**. $C_{32}H_{30}F_6N_8OsP_2$; M = 892.78; monoclinic; space group = $P2(1)/n$; a = 10.6493(5) Å, b = 18.3645(8) Å, c = 34.9814(16) Å, β = 97.3999(11)°, V = 6784.3(5) Å^3; Z = 8; ρ_{calcd} = 1.748 Mg·m^{-3}; $F(000)$ = 3504; crystal size = 0.38 × 0.30 × 0.22 mm^3; λ (Mo Kα) = 0.710 73 Å; T = 150(2) K; μ = 3.923 mm^{-1}; 43 647 reflections collected, 15 565 independent reflections (R_{int} = 0.0556), GOF = 1.032, final $R_1[I > 2\sigma(I)]$ = 0.0393, and wR_2 (all data) = 0.0823.

Single-Crystal X-ray Diffraction Studies. Single-crystal X-ray diffraction studies were measured on a Bruker SMART Apex CCD diffractometer using (Mo Kα) radiation (λ = 0.710 73 Å). The data collection was executed using the SMART program. Cell refinement and data reduction were performed with the SAINT program. The structure was determined using the SHELXTL/PC program and refined using full-matrix least-squares.

■ ASSOCIATED CONTENT

Ⓢ Supporting Information

X-ray crystallographic data file (CIF) of Os(II) complexes **1C**, **2**, and **3**, and results concerning the TD-DFT calculation of three Os(II) complexes **1T**, **1C**, and **3**. This material is available free of charge via the Internet at http://pubs.acs.org.

■ AUTHOR INFORMATION

Corresponding Authors

*E-mail: ychi@mx.nthu.edu.tw. (Y.C.)
*E-mail: chop@ntu.edu.tw. (P.-T.C.)
*E-mail: chc@saturn.yzu.edu.tw. (C.H.C.)

Notes

The authors declare no competing financial interest.

■ ACKNOWLEDGMENTS

This work was supported by the Ministry of Science and Technology of Taiwan, under Grant No. NSC-101-2113-M-007-013-MY3. The computation was conducted at the National Center for High-Performance Computing.

■ REFERENCES

(1) Evans, R. C.; Douglas, P.; Winscom, C. J. *Coord. Chem. Rev.* **2006**, *250*, 2093.
(2) Chou, P.-T.; Chi, Y. *Chem.—Eur. J.* **2007**, *13*, 380.
(3) Williams, J. A. G.; Develay, S.; Rochester, D. L.; Murphy, L. *Coord. Chem. Rev.* **2008**, *252*, 2596.
(4) Rausch, A. F.; Thompson, M. E.; Yersin, H. *J. Phys. Chem. A* **2009**, *113*, 5927.
(5) Rausch, A. F.; Homeier, H. H. H.; Yersin, H. *Top. Organomet. Chem.* **2010**, *29*, 193.
(6) Chi, Y.; Chou, P.-T. *Chem. Soc. Rev.* **2010**, *39*, 638.
(7) Chou, P.-T.; Chi, Y.; Chung, M.-W.; Lin, C.-C. *Coord. Chem. Rev.* **2011**, *255*, 2653.
(8) Kalinowski, J.; Fattori, V.; Cocchi, M.; Williams, J. A. G. *Coord. Chem. Rev.* **2011**, *255*, 2401.
(9) You, Y.; Park, S. Y. *Dalton Trans.* **2009**, 1267.
(10) Zhou, G.; Wong, W.-Y.; Suo, S. *J. Photochem. Photobiol., C* **2010**, *11*, 133.
(11) Xiao, L.; Chen, Z.; Qu, B.; Luo, J.; Kong, S.; Gong, Q.; Kido, J. *Adv. Mater.* **2011**, *23*, 926.
(12) D'Andrade, B. *Nat. Photonics* **2007**, *1*, 33.
(13) Kamtekar, K. T.; Monkman, A. P.; Bryce, M. R. *Adv. Mater.* **2010**, *22*, 572.
(14) Gather, M. C.; Koehnen, A.; Meerholz, K. *Adv. Mater.* **2011**, *23*, 233.
(15) Sasabe, H.; Kido, J. *J. Mater. Chem. C* **2013**, *1*, 1699.
(16) Kaim, W. *Coord. Chem. Rev.* **2011**, *255*, 2503.
(17) Pansare, V. J.; Hejazi, S.; Faenza, W. J.; Prud'homme, R. K. *Chem. Mater.* **2012**, *24*, 812.
(18) Xiang, H.; Cheng, J.; Ma, X.; Zhou, X.; Chruma, J. J. *Chem. Soc. Rev.* **2013**, *42*, 6128.
(19) Borek, C.; Hanson, K.; Djurovich, P. I.; Thompson, M. E.; Aznavour, K.; Bau, R.; Sun, Y.; Forrest, S. R.; Brooks, J.; Michalski, L.; Brown, J. *Angew. Chem., Int. Ed.* **2007**, *46*, 1109.
(20) Ji, S.; Wu, W.; Wu, W.; Song, P.; Han, K.; Wang, Z.; Liu, S.; Guo, H.; Zhao, J. *J. Mater. Chem.* **2010**, *20*, 1953.
(21) Liu, Y.; Hammitt, R.; Lutterman, D. A.; Joyce, L. E.; Thummel, R. P.; Turro, C. *Inorg. Chem.* **2009**, *48*, 375.
(22) Beverina, L.; Salice, P. *Eur. J. Org. Chem.* **2010**, 1207.
(23) Soldatova, A. V.; Kim, J.; Rizzoli, C.; Kenney, M. E.; Rodgers, M. A. J.; Rosa, A.; Ricciardi, G. *Inorg. Chem.* **2010**, *50*, 1135.
(24) You, Y.; Nam, W. *Chem. Soc. Rev.* **2012**, *41*, 7061.
(25) Qian, G.; Wang, Z. Y. *Chem.—Asian J.* **2010**, *5*, 1006.
(26) Ellinger, S.; Graham, K. R.; Shi, P.; Farley, R. T.; Steckler, T. T.; Brookins, R. N.; Taranekar, P.; Mei, J.; Padilha, L. A.; Ensley, T. R.; Hu, H.; Webster, S.; Hagan, D. J.; Van Stryland, E. W.; Schanze, K. S.; Reynolds, J. R. *Chem. Mater.* **2011**, *23*, 3805.
(27) Adams, C. J.; Fey, N.; Weinstein, J. A. *Inorg. Chem.* **2006**, *45*, 6105.
(28) Bennett, M. A.; Bhargava, S. K.; Cheng, E. C.-C.; Lam, W. H.; Lee, T. K.-M.; Priver, S. H.; Wagler, J.; Willis, A. C.; Yam, V. W.-W. *J. Am. Chem. Soc.* **2010**, *132*, 7094.
(29) Rossi, E.; Murphy, L.; Brothwood, P. L.; Colombo, A.; Dragonetti, C.; Roberto, D.; Ugo, R.; Cocchi, M.; Williams, J. A. G. *J. Mater. Chem.* **2011**, *21*, 15501.
(30) Nguyen, M.-H.; Yip, J. H. K. *Organometallics* **2011**, *30*, 6383.
(31) Wu, X.; Liu, Y.; Wang, Y.; Wang, L.; Tan, H.; Zhu, M.; Zhu, W.; Cao, Y. *Org. Electron.* **2012**, *13*, 932.
(32) Sun, Y.; Borek, C.; Hanson, K.; Djurovich, P. I.; Thompson, M. E.; Brooks, J.; Brown, J. J.; Forrest, S. R. *Appl. Phys. Lett.* **2007**, *90*, 213503.
(33) Graham, K. R.; Yang, Y.; Sommer, J. R.; Shelton, A. H.; Schanze, K. S.; Xue, J.; Reynolds, J. R. *Chem. Mater.* **2011**, *23*, 5305.
(34) Damas, A.; Gullo, M. P.; Rager, M. N.; Jutand, A.; Barbieri, A.; Amouri, H. *Chem. Commun.* **2013**, *49*, 3796.
(35) Williams, E. L.; Li, J.; Jabbour, G. E. *Appl. Phys. Lett.* **2006**, *89*, 083506.
(36) Chen, H.-Y.; Yang, C.-H.; Chi, Y.; Cheng, Y.-M.; Yeh, Y.-S.; Chou, P.-T.; Hsieh, H.-Y.; Liu, C.-S.; Peng, S.-M.; Lee, G.-H. *Can. J. Chem.* **2006**, *84*, 309.
(37) Tao, R.; Qiao, J.; Zhang, G.; Duan, L.; Wang, L.; Qiu, Y. *J. Phys. Chem. C* **2012**, *116*, 11658.
(38) Lee, T.-C.; Hung, J.-Y.; Chi, Y.; Cheng, Y.-M.; Lee, G.-H.; Chou, P.-T.; Chen, C.-C.; Chang, C.-H.; Wu, C.-C. *Adv. Funct. Mater.* **2009**, *19*, 2639.
(39) Du, B.-S.; Liao, J.-L.; Huang, M.-H.; Lin, C.-H.; Lin, H.-W.; Chi, Y.; Pan, H.-A.; Fan, G.-L.; Wong, K.-T.; Lee, G.-H.; Chou, P.-T. *Adv. Funct. Mater.* **2012**, *22*, 3491.
(40) Vogler, A.; Kunkely, H. *Top. Curr. Chem.* **2001**, *213*, 143.
(41) Wu, P.-C.; Yu, J.-K.; Song, Y.-H.; Chi, Y.; Chou, P.-T.; Peng, S.-M.; Lee, G.-H. *Organometallics* **2003**, *22*, 4938.
(42) Chang, S.-H.; Chang, C.-F.; Liao, J.-L.; Chi, Y.; Zhou, D.-Y.; Liao, L.-S.; Jiang, T.-Y.; Chou, T.-P.; Li, E. Y.; Lee, G.-H.; Kuo, T.-Y.; Chou, P.-T. *Inorg. Chem.* **2013**, *52*, 5867.

(43) Tung, Y.-L.; Wu, P.-C.; Liu, C.-S.; Chi, Y.; Yu, J.-K.; Hu, Y.-H.; Chou, P.-T.; Peng, S.-M.; Lee, G.-H.; Tao, Y.; Carty, A. J.; Shu, C.-F.; Wu, F.-I. *Organometallics* **2004**, *23*, 3745.
(44) Yeh, H.-H.; Ho, S.-T.; Chi, Y.; Clifford, J. N.; Palomares, E.; Liu, S.-H.; Chou, P.-T. *J. Mater. Chem. A* **2013**, *1*, 7681.
(45) Liao, J.-L.; Chi, Y.; Su, Y.-D.; Huang, H.-X.; Chang, C.-H.; Liu, S.-H.; Lee, G.-H.; Chou, P.-T. *J. Mater. Chem. C* **2014**, *2*, 6269.
(46) Buist, D.; Williams, N. J.; Reibenspies, J. H.; Hancock, R. D. *Inorg. Chem.* **2010**, *49*, 5033.
(47) Hwang, F.-M.; Chen, H.-Y.; Chen, P.-S.; Liu, C.-S.; Chi, Y.; Shu, C.-F.; Wu, F.-I.; Chou, P.-T.; Peng, S.-M.; Lee, G.-H. *Inorg. Chem.* **2005**, *44*, 1344.
(48) Sommer, J. R.; Shelton, A. H.; Parthasarathy, A.; Ghiviriga, I.; Reynolds, J. R.; Schanze, K. S. *Chem. Mater.* **2011**, *23*, 5296.
(49) Yao, L.; Zhang, S.; Wang, R.; Li, W.; Shen, F.; Yang, B.; Ma, Y. *Angew. Chem., Int. Ed.* **2014**, *53*, 2119.
(50) Su, S.-J.; Tanaka, D.; Li, Y.-J.; Sasabe, H.; Takeda, T.; Kido, J. *Org. Lett.* **2008**, *10*, 941.
(51) Tse, S. C.; Kwok, K. C.; So, S. K. *Appl. Phys. Lett.* **2006**, *89*, 262102.
(52) Hamada, Y.; Kanno, H.; Tsujioka, T.; Takahashi, H.; Usuki, T. *Appl. Phys. Lett.* **1999**, *75*, 1682.
(53) Chang, C.-H.; Lin, Y.-H.; Chen, C.-C.; Chang, C.-K.; Wu, C.-C.; Chen, L.-S.; Wu, W.-W.; Chi, Y. *Org. Electron.* **2009**, *10*, 1235.
(54) Tung, Y.-L.; Lee, S.-W.; Chi, Y.; Tao, Y.-T.; Chien, C.-H.; Cheng, Y.-M.; Chou, P.-T.; Peng, S.-M.; Liu, C.-S. *J. Mater. Chem.* **2005**, *15*, 460.
(55) Chou, P.-T.; Yu, W.-S.; Cheng, Y.-M.; Pu, S.-C.; Yu, Y.-C.; Lin, Y.-C.; Huang, C.-H.; Chen, C.-T. *J. Phys. Chem. A* **2004**, *108*, 6487.

dx.doi.org/10.1021/ic501474r | *Inorg. Chem.* 2014, 53, 9366−9374